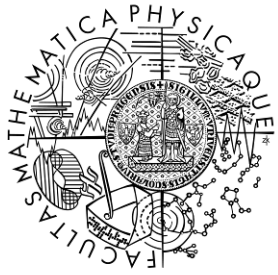

FACULTY
OF MATHEMATICS
AND PHYSICS
Charles University

THESIS

Eva Butková

Spectroscopic studies of new generation of optical and magneto-optical materials

Institute of Physics of Charles University

Supervisor of the doctoral thesis: RNDr. Martin Veis, Ph.D.

Study programme: Quantum Optics and Optoelectronics

Prague 2020

Introduction

In recent decades, technology has become smaller, faster, and more effective than ever. However, there is still a room for improvement, which has been demonstrated by multiple novel devices proposed by scientific community, such as 3D holographic displays, magnetic recording, optical isolators and circulators, high-energy X-ray/gamma ray detectors and many more. This kind of novel technology, usually operates in nanoscale. However, nanoscale materials are not only difficult to prepare but their physical properties may also significantly differ from physical properties of their bulk forms. Therefore, the knowledge from the bulk material research can be used only to some extent. What is more, physical properties of materials in nanoscale are significantly influenced by surrounding materials (for example in a multilayer). This goes hand in hand with the requirement of compatibility with the current technology (usually Si compatibility) which is particularly important. In addition, the huge variety of proposed highly specialized devices requires materials with tunable optical, magnetic, and magneto-optical (MO) properties. This type of tuning is usually performed by doping, composition or/and application of strain. These mechanisms must therefore be also understood and thoroughly researched.

To process all these inputs properly, one must come up with a parameter which characterizes optical and MO properties of studied materials completely. Moreover, this parameter must fully represent studied materials (together with the dimensions information) in any optical or MO calculation. The only parameter which meets all these requirements is the permittivity tensor. Knowledge of the permittivity tensor spectra allows deep understanding of the optical and MO properties of the material. Furthermore, when combined with Yeh 4x4 matrix formalism, it allows calculations of interaction between electromagnetic radiation and multilayered structure.

For all these reasons combined, we devoted present work to the full permittivity tensor determination and analysis. This was done for three groups of promising novel materials:

- $Gd_xFe_{(100-x)}$ (GdxFe)
- magnetic garnets: $Y_{3-x}Bi_xFe_5O_{12}$ (Bix:YIGs); $Nd_2BiFe_{(5-x)}Ga_xO_{12}$ (Bi1:NIGxGs) and $Nd_{0.5}Bi_{2.5}Fe_{(5-x)}Ga_xO_{12}$ (Bi2.5:NIGxGs)

- $Ce_{(0.95-x)}Hf_xCo_{0.05}O_{(2-\delta)}$ (CeHfxCoO)

To tune their physical properties properly, we investigated the influence of the material composition as well.

Theory

We can describe the behavior of electromagnetic waves in a material by permittivity and permeability tensors. At optical frequencies, we can take magnetic permeability as unity. If we are working with a cubic crystal and magnetization parallel to the z-axis of the Cartesian coordinate system (the magnetic film-ambient interface is normal to the z-axis), the dielectric permittivity tensor has the form

$$\varepsilon = \begin{pmatrix} \varepsilon_1 & -i\cdot\varepsilon_2 & 0 \\ i\cdot\varepsilon_2 & \varepsilon_1 & 0 \\ 0 & 0 & \varepsilon_3 \end{pmatrix}. \qquad (1)$$

We restricted ourselves to linear MO effects, which implies $\varepsilon_3=\varepsilon_1$. All elements of the tensor have a real and imaginary part:

$$\begin{aligned} \varepsilon_1 &= \varepsilon_{1r} - i\cdot\varepsilon_{1i} \\ \varepsilon_2 &= \varepsilon_{2r} - i\cdot\varepsilon_{2i} \end{aligned}. \qquad (2)$$

We can describe optical behavior of the sample, upon the light reflection and transmission, in the base of s and p polarization components by Jones reflection and transmission matrices where the matrix elements are the amplitude reflection and transmission coefficients for the s and p polarized waves.

$$J_{sp}^R = \begin{pmatrix} r_{ss} & r_{sp} \\ r_{ps} & r_{pp} \end{pmatrix} J_{sp}^I, \qquad J_{sp}^T = \begin{pmatrix} t_{ss} & t_{sp} \\ t_{ps} & t_{pp} \end{pmatrix} J_{sp}^I. \qquad (3)$$

We can derive diagonal elements of the permittivity tensor from the Spectroscopic Ellipsometry (SE) data analysis. The change in the polarization state of the reflected beam can be expressed by ellipsometric Psi (ψ) and Delta (Δ) parameters defined by the equation:

$$\tan\psi \cdot e^{i\Delta} = \rho = \frac{r_{pp}}{r_{ss}} . \quad (4)$$

In this equation, tanψ is the magnitude of the reflectivity ratio and Δ is the phase. The r_{pp} and r_{ss} are amplitude reflection coefficients for s and p polarization measured from the alternating current (AC) signal [1]. In order to increase the information content when measuring absorbing thin film on transparent substrate it is a common approach to supplement the SE data with intensity transmission data (transmitted intensity is calculated from the AC signal). The important step in the SE analysis is the proper parametrization of the dispersion of the unknown optical functions ε_{1r} and ε_{1i}. In this work, we used Kramers-Kronig (KK) consistent Gaussian, Lorentz and Drude parameterization.

Gaussian oscillator produces Gaussian line shape in ε_{1i}:

$$\varepsilon_{1\_Gaussian} = Amp\left\{\begin{array}{l}\left(\Gamma\left(\frac{E-E_0}{\sigma}\right)+\Gamma\left(\frac{E+E_0}{\sigma}\right)\right)+ \\ i\cdot\left(\exp\left[-\left(\frac{E-E_0}{\sigma}\right)^2\right]+\exp\left[-\left(\frac{E+E_0}{\sigma}\right)^2\right]\right)\end{array}\right\}, \quad (5)$$

$$\sigma = \frac{Br}{2\sqrt{\ln(2)}} . \quad (6)$$

The function Γ is a convergence series that produces a KK consistent line shape for ε_{1r} [1, 2].

Classic version of Lorentz oscillator is:

$$\varepsilon_{1\_Lorentz} = \frac{AmpBrE_0}{E_0^2 - E^2 - i\cdot EBr} . \quad (7)$$

Parameters E_0, Amp, Br denote the center energy, amplitude and the broadening parameter respectively [1, 3].

As a common approach, we used Drude model to describe the free carrier effect on the dielectric response:

$$\varepsilon_{1\_Drude} = \frac{-\hbar^2 q^2 N\mu}{\varepsilon_0(\mu m^* m_e E^2 + iq\hbar E)} . \quad (8)$$

Parameters N, μ, m* denote the carrier concentration, carrier mobility and carrier effective mass respectively. The physical constants are ħ (Planck constant/2π), q (electron charge), ε_0 (the vacuum dielectric constant) and m_e (the electron mass) [1, 4].

Knowledge of the diagonal elements of the permittivity tensor allows to derive the off-diagonal elements using a combination of MOKE and Faraday spectra along with the theoretical calculations. These calculations are based on Yeh's 4x4 matrix formalism [5]. We can express the change in a polarization state of the light upon reflection/transmission by the complex Kerr MO angle Φ_K and the complex Faraday MO angle Φ_F. For p-polarized incident light we define them as follows

$$\Phi_K = \theta_K - i \cdot e_K = \frac{r_{sp}}{r_{pp}}, \tag{9}$$

$$\Phi_F = \theta_F - i \cdot e_F = -\frac{t_{sp}}{t_{pp}}. \tag{10}$$

In these equations Θ_k is the Kerr rotation, e_k is the Kerr ellipticity, Θ_F is the Faraday rotation and e_F is the Faraday ellipticity. Let us consider the case of a 2 layered medium, where the first layer is a bulk substrate and the second layer is a thin film. We will work in Cartesian coordinates where the sample interface is perpendicular to the z-axis, the wave vector of the incident light is perpendicular to the x-axis and each layer is characterized by a complex permittivity tensor and a thickness. In this case, Yeh Matrix Formalism allows to express the relationship between the electric field amplitudes on the substrate/film interface ($E_0^{(0)}(z)$) and the electric field amplitudes on the film/ambient interface ($E_0^{(2)}(z_1)$) as

$$E_0^{(0)}(z) = [D^{(0)}]^{-1} D^{(1)} P^{(1)} [D^{(1)}]^{-1} D^{(2)} E_0^{(2)}(z_1) = M E_0^{(2)}(z_1). \tag{11}$$

Superscripts in brackets, n = 0, 1 and 2 are markers of the substrate (0), thin film (1) and the ambient half space (2). P stands for propagation and D for dynamical matrix respectively [5].

We can interpret the full permittivity tensor in terms of microscopic theory which relates its spectra to energy-level splitting and transition probabilities. In this work, we will consider two types; double and single transitions [6, 7].

Double transitions refer to spin and electric-dipole allowed transitions between an orbital singlet ground state and an excited state which is split by the combined effect of exchange field and spin-orbit coupling. For these transitions ε_2 behaves as:

$$\varepsilon_2 = \frac{\omega_p^2 f \Delta L}{2\omega_0} \frac{(\omega_0 - \omega)^2 - \Gamma_0^2 + 2i\Gamma_0(\omega_0 - \omega)}{\left[(\omega_0 - \omega)^2 + \Gamma_0^2\right]^2} \qquad (12)$$

In this equation, Δ is the separation between the levels caused by spin-orbit coupling, ω_0 is the center frequency, Γ_0 is the half width at half-height of the transition and f is the oscillator strength. L is the Lorentz-Lorentz local field correction, n is the refraction index.

In the case of single transitions neither the ground state nor the final state are split but the oscillator strengths for right circularly polarized light f_+ and left circularly polarized light f_- are different. In this case ε_2 behaves as:

$$\varepsilon_2 = \frac{\omega_p^2 f df L}{2} \frac{\omega(\omega_0^2 - \omega^2 - \Gamma_0^2) - i\Gamma_0(\omega_0^2 + \omega^2 + \Gamma_0^2)}{\omega_0\left[(\omega_0^2 + \omega^2 + \Gamma_0^2)^2 + 4\omega^2\Gamma_0^2\right]^2}, \qquad (13)$$

Where df is the fractional dichroism [6, 7].

In our SE, MOKE and Faraday effect analysis, we considered surface roughness which was for each sample represented by a thin layer with a permittivity given by Effective Medium Approximation formula (EMA) [8]. EMA creates an effective dielectric permittivity ε_{eff} for a system made up of inclusions of a material with dielectric permittivity ε_m in a material with dielectric permittivity ε_h.

$$(f-1)\frac{\varepsilon_h - \varepsilon_{eff}}{\varepsilon_{eff} + D(\varepsilon_h - \varepsilon_{eff})} = f\frac{\varepsilon_m - \varepsilon_{eff}}{\varepsilon_{eff} + D(\varepsilon_m - \varepsilon_{eff})}. \qquad (14)$$

In this formula f denotes the volume fraction of the ε_m material inclusions ($f \in (0, 1)$) and D stands for depolarization fixed to 1/3, which corresponds to spherical inclusions.

Resutls

1. GdxFe

Amorphous ferrimagnetic thin films composed of rare earth and transition metals attracted considerable attention because of their useful technological applications [9-12]. As one of theirs important representative, GdxFe has significant advantages, such as large magnetization density, and possibility to adjust its compensation temperature, coercive and saturation magnetization by changing the composition [13-15]. Another valuable feature of GdxFe is that it enables direct access to its spins through the electromagnetic interactions. Such feature makes this material subject of importance for future magnetic recording (such as heat assisted magnetic recording) and information processing technologies. Recently, a novel concept of high speed MO spatial light modulator (MO-SLM) for holographic displays based on giant magnetoresistance with GdxFe as a free layer was proposed [10]. When using GdxFe for MO-SLM driven by spin transfer torque, it is particularly important that GdxFe shows perpendicular anisotropy. This happens when the Fe concentration is close to the compensation concentration, which is for this material about 75% [16]. When GdxFe acts as a free layer, it is especially important to control its composition precisely, since it significantly affects its magnetic switching property. Coercivity shows maxima when the GdxFe composition is the compensation one, and it gets smaller when the composition becomes Fe rich (compared to the compensation composition). Spin-torque switching current of the spin MO-SLM is significantly reduced with an increase in Fe concentration and it shows very small switching current when composition is slightly Fe richer than the compensation one [17, 18]. Therefore, it is meaningful to investigate optical properties of the GdxFe material around the compensation concentration.

a) **Samples:** We focused on GdxFe thin films (x=18.3, 20, 24.7, 26.7) prepared on thermally oxidized silicon substrate. We used Ru and SiO_2 as coating layers. We deposited GdxFe and Ru coating by direct current sputtering technique in Kr gas of pressure 8.7x10-2 Pa with a deposition rate of 3.6 nm/min. We deposited SiO_2 coating by ion beam sputtering technique with radio frequency ion source. Model structures of our samples are shown in Figure 1.
b) **Spectroscopic Ellipsometry:** We measured ellipsometry Psi and Delta parameters of the reflected light in the spectral range from 1.3 to 5.5 eV for incident angles 55°, 60° and

65°. Obtained experimental data were analyzed using CompleteEase software. From this analysis, we derived the diagonal permittivity tensor elements.

c) **MOKE spectroscopy:** We obtained the MOKE rotation and ellipticity spectra in the polar configuration. We acquired all the spectra at the room temperature for nearly normal light incidence. Applied magnetic field was 1.2 T, which was enough for magnetic saturation of samples. Incident light was *s* polarized. We recorded data in the photon energy range from 1.5 to 5.5 eV. Using a combination of the SE and MO measurements we determined the spectral dependence of off-diagonal permittivity tensor elements. We also performed MOKE hysteresis measurements. We measured MOKE rotation hysteresis loops by differential intensity detection method at 2.38 eV. We performed all measurements in the polar geometry and at the room temperature. Field was ranging from -1.8 mT up to 1.8 mT, which was far beyond saturation point.

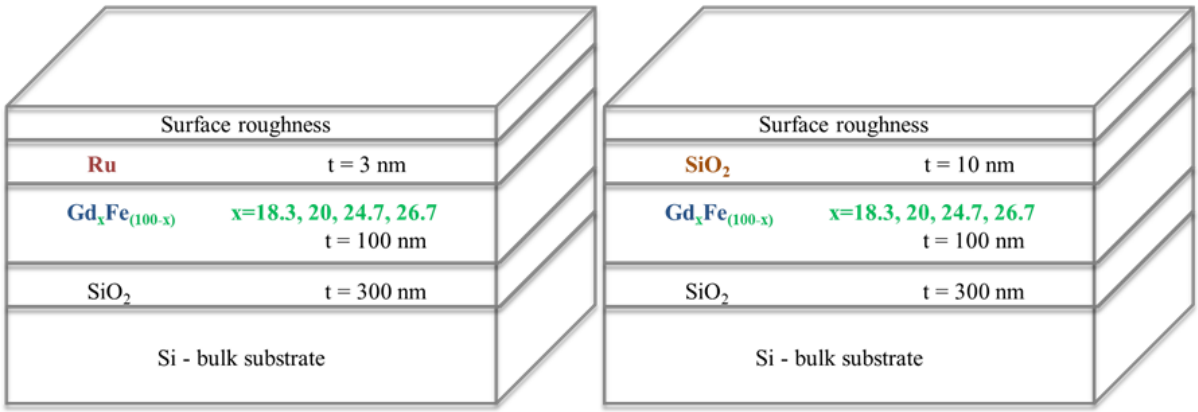

Figure 1: Model structure of GdxFe/Ru and GdxFe/SiO_2 samples used for SE and MOKE analysis calculations.

In this work, we determined complete permittivity tensors of GdxFe with various compositions (x=18.3, 20, 24.7, 26.7) in the spectral range from 1.5 to 5.5 eV (Figure 2 and Figure 3). We parameterized obtained results in terms of microscopic theory which relates permittivity tensor spectra to the energy-level splitting and transition probabilities. Our investigation showed that the ε_{1r} behavior in the spectral range from 1.5 to 3 eV, where ε_{1r} decreases its value for higher energies (Figure 2), differs from a typical Drude-like behavior (describing intra-band transitions) of metallic compounds. On the other hand, it is like the behavior of some transition metals (Cr, Gd, Ru, Ti [19, 20]). This is caused by the Lorentz contribution centered near 1.9 eV. This contribution most likely originates from the inter-band transition, which involves Fe 3d and Gd 5d states. The Fe 3d state is located around 1.5 eV below Fermi energy. Contrarywise, Gd 5d states are located approx. 0.5 eV above the Fermi energy. The second Lorentz oscillator near 2.5 eV does not significantly modify the

spectral dependence of the Drude behavior. The reason is its small amplitude. This points on the origin of Gd d-d electron transition, since this transition should be forbidden with small oscillator strength. Finally, we discuss the Gd substitution effect. The amplitude of the first Lorentz oscillator near 1.9 eV decreases with Gd content. Increasing Gd content means decreasing Fe density of states below Fermi energy. This results in the suppression of Fe 3d to Gd 5d transition probability. On the contrary, the increase of Gd content is increasing the amplitude of the second Lorentz oscillator centered near 2.5 eV. Such behavior supports the assignment of the origin to Gd d-d transition. Our investigation of MO properties of GdxFe showed that Gd substitution decreases both, ε_{2r} and ε_{2i} amplitudes (Figure 3). We attributed this to the fact that the magnetic moment of Fe is in this ferrimagnetic alloy stronger than the magnetic moment of Gd. Perpendicular anisotropy of GdxFe was confirmed for all the samples (Figure 4). Moreover, we observed change in the magnetization direction to the opposite site when reaching the compensation concentration. We used one Dia transition to parameterize spectra of the off-diagonal elements of the GdxFe permittivity tensor in terms of microscopic theory. We assumed that the MO effect comes from different probabilities of transition between an orbital singlet ground state and split excited state and that Gd concentration decreases this splitting.

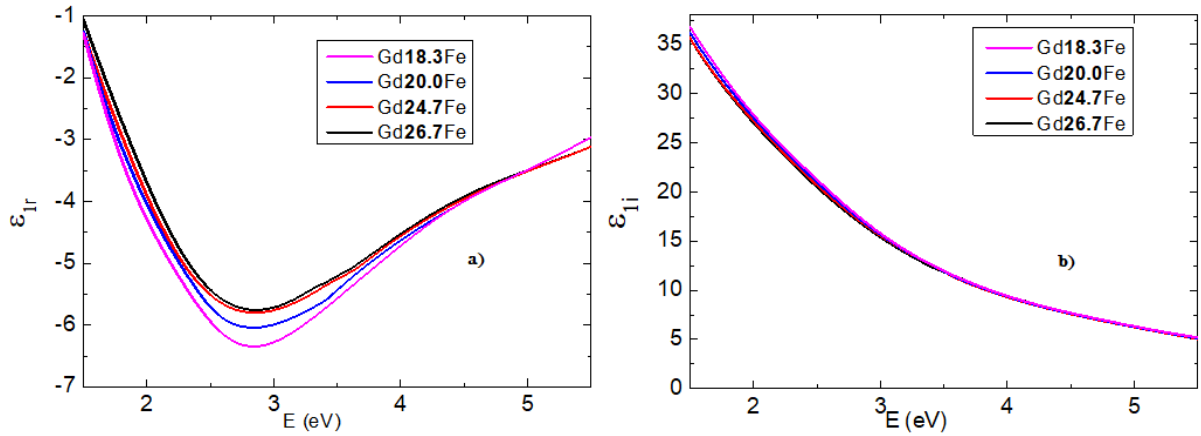

Figure 2: a) Real parts of the diagonal elements of the permittivity tensors of GdxFe thin films. b) Imaginary parts of the diagonal elements of the permittivity tensors of GdxFe.

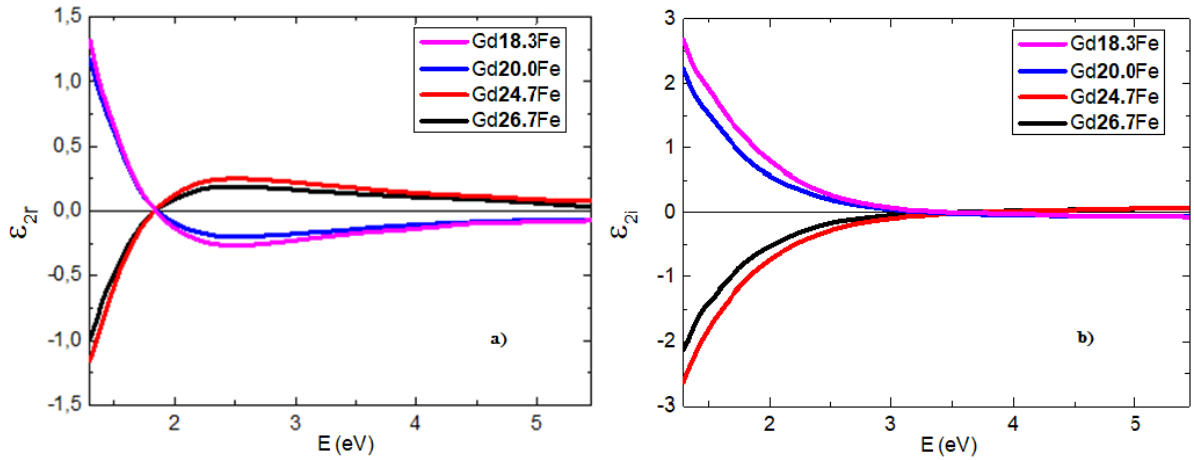

Figure 3: a) Real parts of the off-diagonal elements of the permittivity tensors of GdxFe. b) Imaginary parts of the off-diagonal elements of the permittivity tensors of GdxFe.

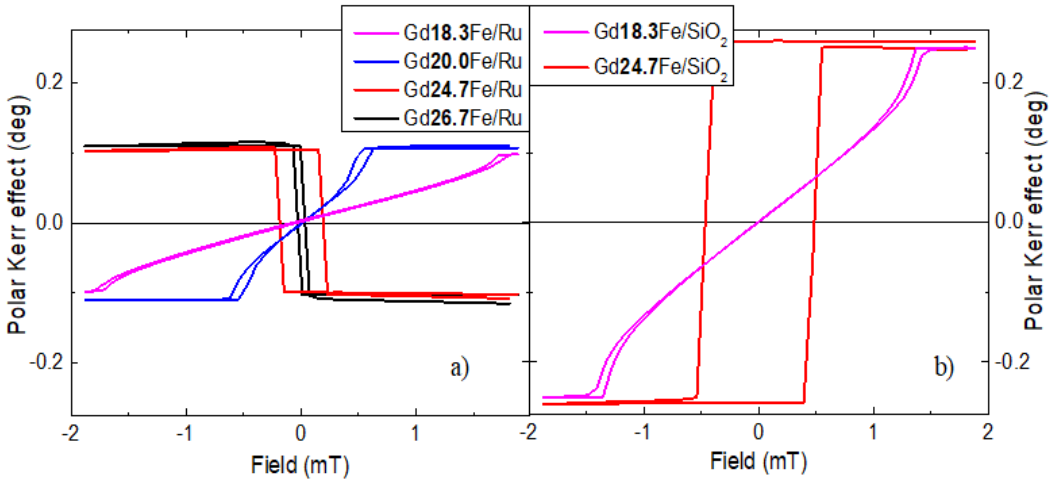

Figure 4: Hysteresis loops of examined GdxFe samples with a) Ru and b) SiO_2 coatings at 2.38 eV.

2. *Magnetic garnets*

Magnetic garnets are complex crystalline materials. These materials have recently attracted a considerable attention as they have high application potential. This is manly given by several magneto-electric, spintronic and MO phenomena, such as spin Seebeck effect [21], spin Hall magneto-resistance [22] as well as high MOKE and Faraday effect in the visible-light region. In this work, we focus on bismuth substituted yttrium iron garnets Bix:YIGs; as well as on bismuth and gallium substituted neodymium iron garnets Bi1:NIGxGs and Bi2.5:NIGxGs. Both materials exhibit strong spin-orbit coupling enhanced by 6p orbitals of Bi. Furthermore, Bi1:NIGxGs and Bi2.5:NIGxGs exhibit strong out-of-plane magnetic anisotropy achieved by Ga substitution and crystal orientation (111) of the $Gd_3Ga_5O_{12}$ (GGG) substrate. Currently, people use various techniques to grow magnetic garnet thin films of high optical and MO

quality. Metal Organic Decomposition (MOD), used in this work, has been demonstrated as a very promising method for this type of material.

2.1 Bix:YIGs

a) **Samples:** We focused on Bix:YIGs thin films (x= 1.5, 2, 2.5, 3) prepared on GGG (100) substrates. The thin films were prepared by MOD method. MOD liquids for garnet films consisted of solutions made of Bi, Y, and Fe carboxylates. The total concentration of carboxylates was 3 – 4% [23, 24]. Model structures of our samples are shown in Figure 5.

b) **Spectroscopic Ellipsometry:** We performed SE measurements on a Mueller matrix ellipsometer Woollam RC2. We measured spectral dependence of ellipsometry parameters ψ and Δ in reflection and at incident angles 55°, 60° and 65°. We used the same equipment to measure the transmission spectra at the incidence angle 0°. All measurements were performed in the spectral range from 1.5 to 6.5 eV. We analyzed SE experimental data using a CompleteEase software provided by WoollamCo.. We used multi sample analysis (MSA) mode to obtain the diagonal elements of the permittivity tensor ε_{1r} and ε_{1i} of GGG and Bix:YIGs materials. MSA is an advanced mode that allows simultaneous fit of data from multiple samples [1]. In MSA mode, we combined ellipsometry and transmission measurements for each material. We used transmission spectra because of the strong interference observed in ψ and Δ in the transparent spectra region below 2.5 eV. We fitted the SE and transmission experimental data using model structure shown in Figure 5.

c) **MOKE and Faraday effect spectroscopy:** We measured MOKE rotation and ellipticity spectra in the polar configuration. We acquired the spectra at room temperature and at nearly normal light incidence. Applied magnetic field was 1.2 T which was enough for samples saturation. We used p-polarized light. We recorded data in the photon energy range from 1.4 to 5 eV. Faraday rotation and ellipticity spectra were acquired at room temperature using magnetic field 665 mT, which was enough for samples saturation. We recorded Faraday experimental spectra in the photon energy range from 1.4 to 4 eV. Faraday hysteresis loops were measured at 3 eV. Using a combination of the SE and MO measurements we determined the spectral dependence of the off-diagonal permittivity tensor elements.

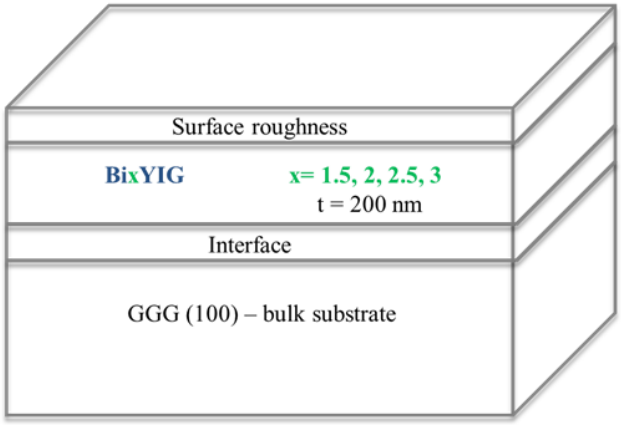

Figure 5: Model structure of Bix:YIGs samples used for SE, MOKE and Faraday analysis calculations.

In this work, we determined complete permittivity tensors of Bix:YIGs thin films with various Bi concentrations (x=1.5, 2, 2.5, 3) in the spectral range from 1.5 to 5 eV. We parameterized obtained results in terms of microscopic theory. Permittivity tensor spectra analysis showed that bismuth substitution increases amplitudes of ε_{1r} and ε_{1i} in the measured spectral range (Figure 6). We observed optical transitions at 2.5, 3.2 and 4.4 eV and the absorption edge near 2.1 eV. As expected, we found that Bi substitution leads to the enhancement in MOKE and Faraday effects which is crucial for the garnet application potential. This result is also connected to the fact that bismuth increases ε_{2r} and ε_{2i} amplitudes at their extremes significantly (Figure 7). We used two Para transitions and three Dia transition to parameterize ε_{2r} and ε_{2i} in terms of microscopic theory. We found that Bi substitution increases amplitudes of almost all transitions. It however lowers energy of Dia transition at 4.65 eV which most likely exists due to the charge transfers from oxygen to octahedral Fe. We associated strongest Dia transitions at 2.5 eV and 3.3 eV with transitions t2(Fe3+) → t2g(Fe2+) and eg(Fe3+) → e(Fe2+). These are mainly responsible for the increase in MO effects. We attributed positive impact of Bi on these transitions to the increase in super-exchange interaction caused by the enhancement of the electronic exchange.

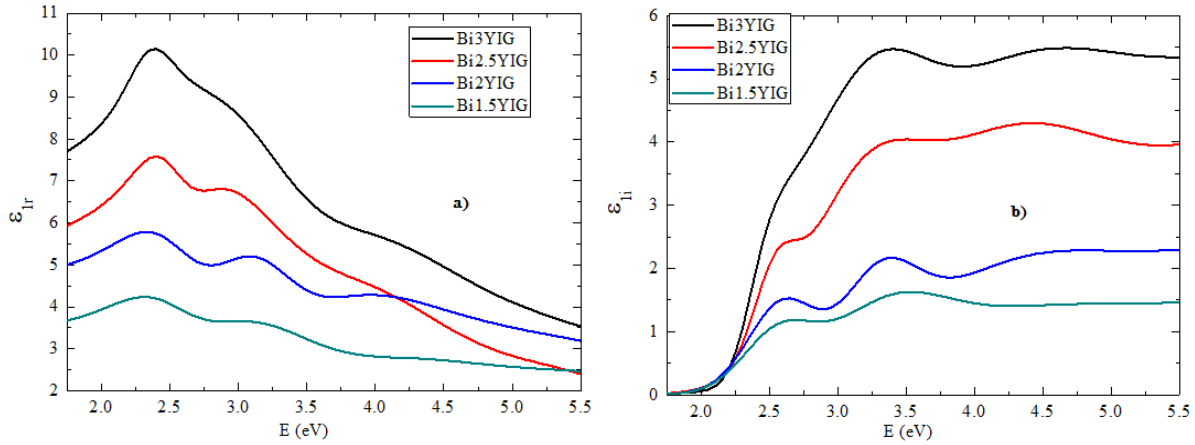

Figure 6: a) Real parts of the diagonal elements of the permittivity tensors of Bix:YIGs. b) Imaginary parts of the diagonal elements of the permittivity tensors of Bix:YIGs.

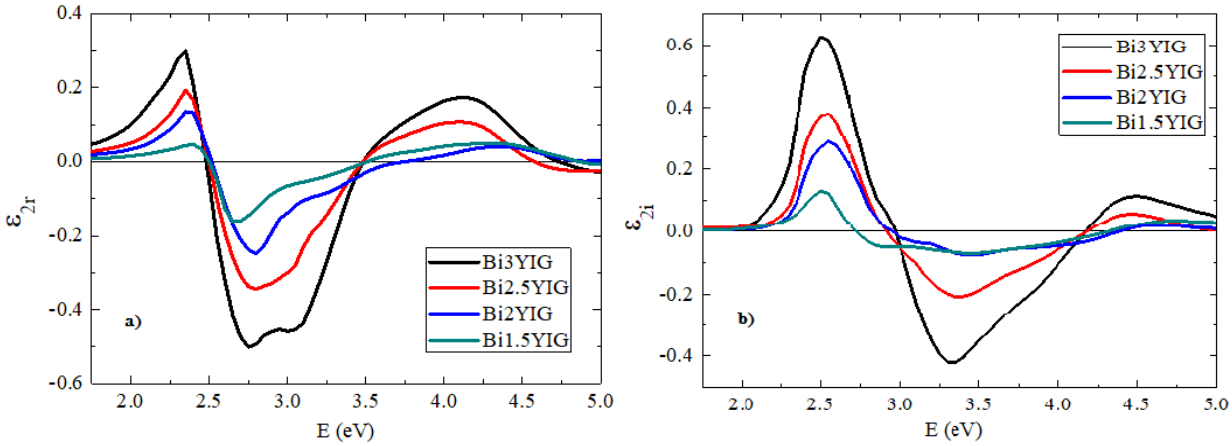

Figure 7: a) Real parts of the off-diagonal elements of the permittivity tensors of Bix:YIGs. b) Imaginary parts of the off-diagonal elements of the permittivity tensors of Bix:YIGs.

2.2 Bi1:NIGxGs and Bi2.5:NIGxGs

a) **Samples:** We focused on Bi1:NIGxGs and Bi2.5:NIGxGs thin films (x = 0, 0.25, 0.75, 1) prepared by MOD method on $Gd_3Ga_5O_{12}$ (GGG) (111) substrates. MOD liquids for garnet films consisted of solutions made of Nd, Bi, Ga, and Fe carboxylates [23, 24]. Model structures of our samples are shown in Figure 8.

b) **Spectroscopic Ellipsometry:** We performed SE measurements on a Mueller matrix ellipsometer Woollam RC2. We measured spectral dependence of ellipsometry parameters ψ and Δ in reflection and at incident angles 55°, 60° and 65°. We used the same equipment to measure the transmission spectra at the incidence angle 0°. We performed measurements in the spectral range from 1.5 to 6.5 eV. We analyzed SE experimental data using a CompleteEase software provided by WoollamCo.. We used

MSA mode to obtain diagonal elements of the permittivity tensor ε_{1r} and ε_{1i} of Bi1:NIGxGs and Bi2.5:NIGxGs.

c) **MOKE and Faraday effect spectroscopy:** We studied MO properties by MOKE and MO Faraday effect spectroscopy. We measured spectra of polar MOKE rotation and ellipticity at room temperature at nearly normal light incidence. We applied magnetic field 1.2 T, which was enough for samples saturation. Incident light was p polarized. We recorded data in the photon energy range from 1.4 to 5 eV. Similarly, we measured spectra of Faraday rotation and ellipticity at room temperature using magnetic field 670 mT (enough for samples saturation). We recorded experimental data in the photon energy range from 1.4 to 4 eV. Using the combination of the SE and MO measurements we determined the spectral dependence of off-diagonal permittivity tensor elements.

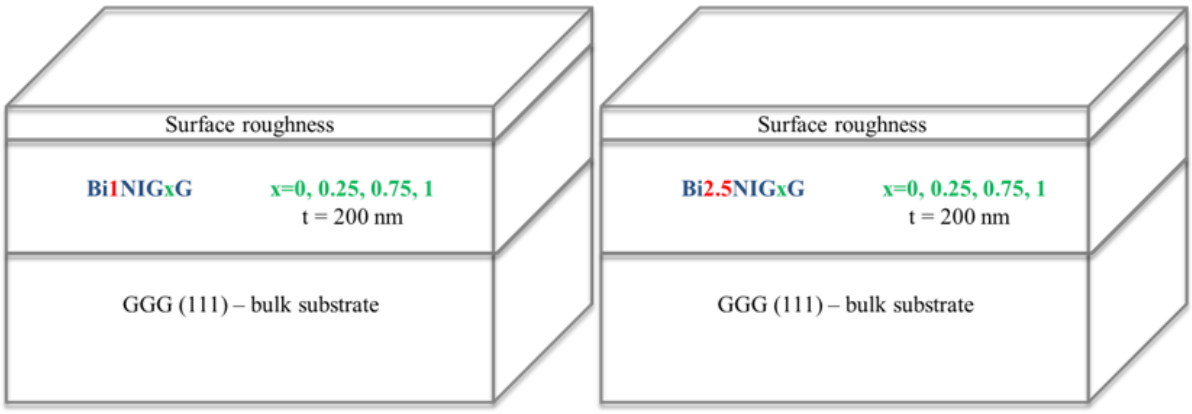

Figure 8: Model structure of Bi1NIGG and Bi2.5NIGG samples used for SE, MOKE and Faraday analysis calculations.

In this work, we determined complete permittivity tensors of Bi1:NIGxGs and Bi2.5:NIGxGs thin films with various Ga concentrations (x=0, 0.25, 0.75, 1) in the spectral range from 1.5 to 5.5 eV. We parameterized obtained results in terms of microscopic theory. Our analysis showed that Ga substitution decreases amplitudes of ε_{1r} for Bi1:NIGxGs below 4 eV and increasing them above. On the other hand, Ga substitution does not noticeably influence amplitudes of ε_{1r} for Bi2.5:NIGxGs. We found that Ga substitution increases an absorption of Bi1:NIGxGs. However, it decreases an absorption of Bi2.5:NIGxGs. Furthermore, the absorption of Bi2.5:NIGxGs is almost 30% stronger than the absorption of Bi1:NIGxGs. We attribute this to the higher Bi concentration. When looking at MO properties, we found that Bi substitution increases, and Ga substitution decreases amplitudes of MO effects. This is connected to ε_{2r} and ε_{2i} amplitudes which are increased by Bi and decreased by Ga substitution. To explain the effect of Ga properly, we parameterized ε_{2r} and ε_{2i} spectra by four

Para transitions to represent crystal field transitions. We also used four Dia transitions. The main contribution comes from Dia transitions, associated with transitions t2(Fe3+) → t2g(Fe2+) and eg(Fe3+) → e(Fe2+), mainly responsible for the remarkable increase in MO effects. We found that Ga substitution decreases these transitions. This is in accordance with the assumption, that Ga is mostly substituted for Fe3+ tetrahedral, which is crucial for both transitions. We also found that Ga substitution lowers energy of much smaller Dia transition at 4.65 eV, which most likely exists due to charge transfers from oxygen to octahedral Fe. This is in accordance with the assumption that Ga is in a smaller percentage also substituted per Fe3+ octahedral.

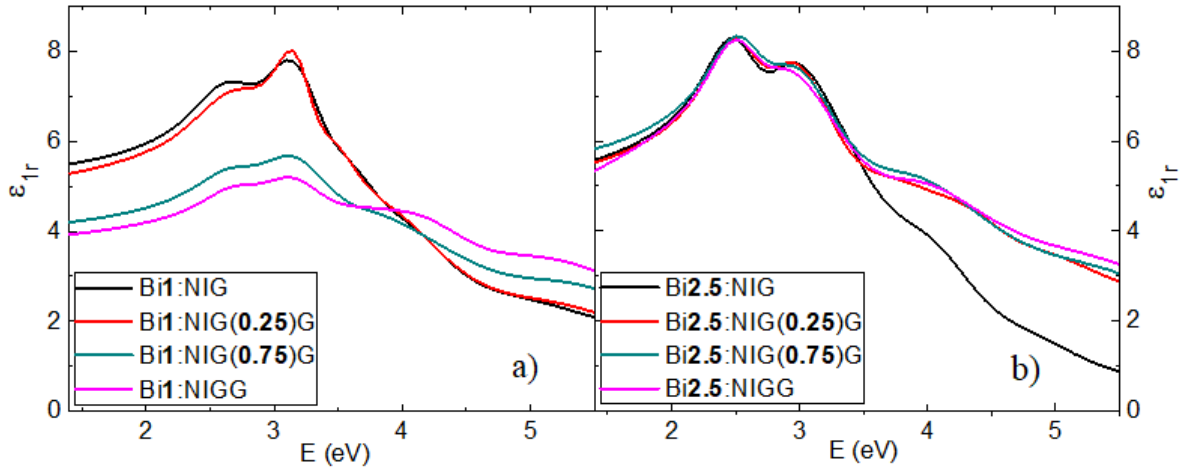

Figure 9: Real parts of the diagonal permittivity tensor elements ε_{1r} of a) Bi1:NIGxGs and b) Bi2.5:NIGxGs.

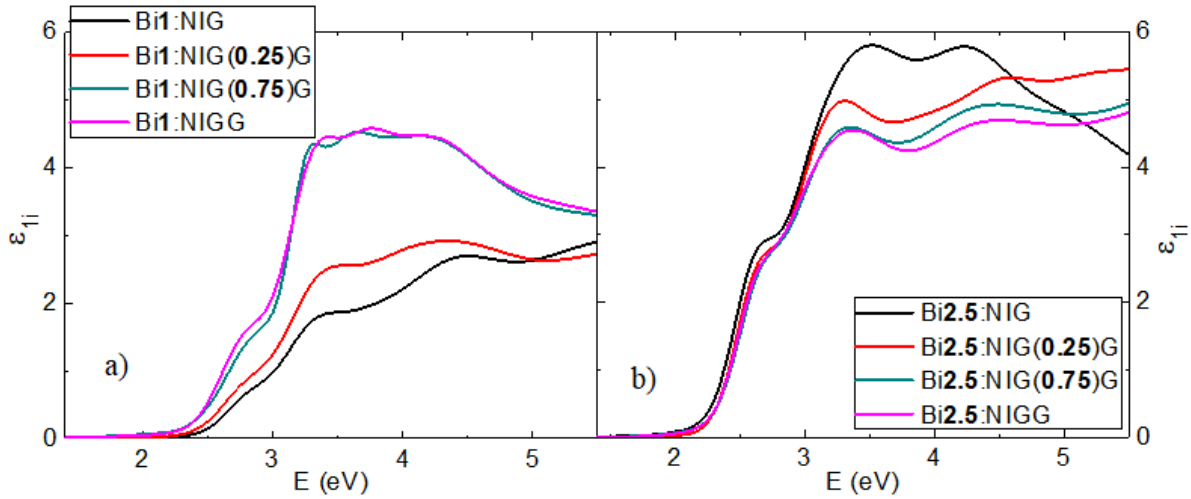

Figure 10: Imaginary parts of the diagonal permittivity tensor elements ε_{1i} of a) Bi1:NIGxGs and b) Bi2.5:NIGxGs.

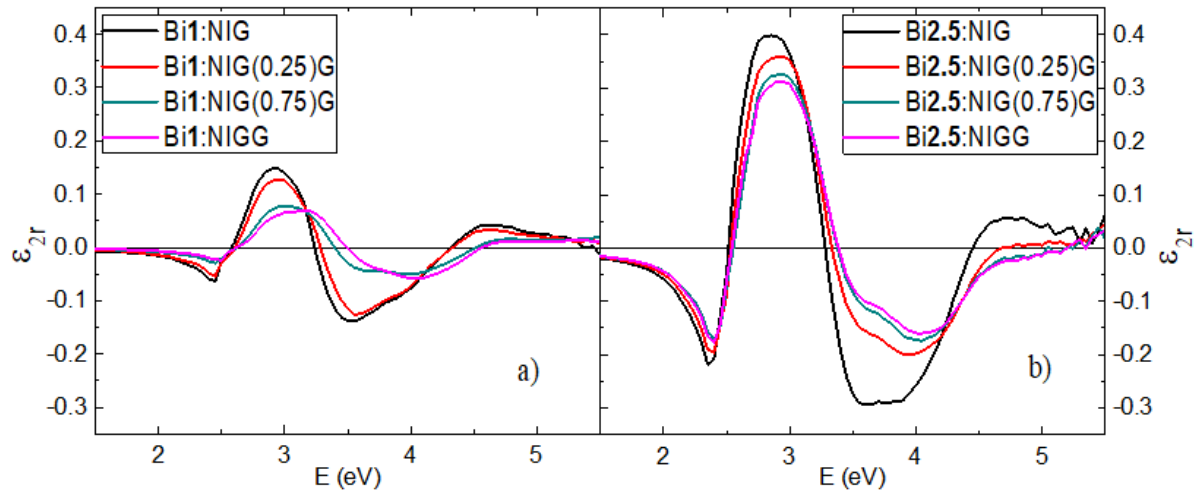

Figure 11: Real parts of the off-diagonal permittivity tensor elements ε_{2r} of a) Bi1:NIGxGs and b) Bi2.5:NIGxGs.

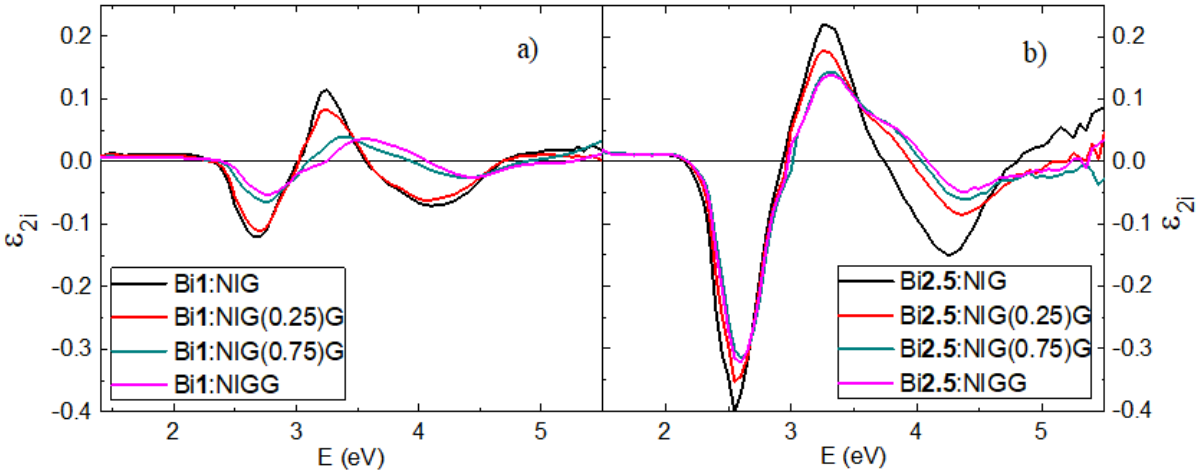

Figure 12: Real parts of the off-diagonal permittivity tensor elements ε_{2r} of a) Bi1:NIGxGs and b) Bi2.5:NIGxGs.

3. *CeHfxCoO*

In recent years, magnetically doped CeO_2 attracted a lot of attention since it is a promising magnetic semiconductor and highly applicable material in the field of integrated photonics. This ranges from MO applications such as integrated MO isolators or magneto-plasmonic sensors to magneto-photonic crystals [25-28]. The main advantage of this material is its high Curie temperature and more importantly a great Si compatibility [29]. Moreover, it is possible to tune CeO_2 magnetic properties by doping of the non-magnetic lattice by magnetic ions [25]. In this work, we used Hf and Co doping. Successful adoption of this material in

MO devices requires complete understanding of the nature and origin of CeO_2 magnetic properties. Even though is the room temperature ferromagnetism in this material explained by an oxygen vacancy mechanism [30, 31], the detail optical and MO analysis is still needed.

a) **Samples:** We studied polycrystalline CeHfxCoO thin films (x = 0, 0.15, 0.35, 0.475, 0.6, 0.8, 0.95) prepared by pulsed laser deposition method on 2 types of substrates: amorphous quartz and Si/SiO_2. The deposition was carried out in vacuum (at base pressure $1.0x10^{-6}$ Torr) with substrate temperature of 700^0C. Figure 13 shows theoretical model structure of CeHfxCoO samples used for SE and Faraday effect analysis.
b) **Spectroscopic Ellipsometry:** We performed SE measurements on a Mueller matrix ellipsometer Woollam RC2. We measured spectral dependence of ellipsometry parameters ψ and Δ in reflection and at incident angles 55°, 60° and 65°. We used the same equipment to measure the transmission spectra of CeHfxCoO thin films prepared on transparent amorphous quartz substrates and we used incidence angle 0°. We performed measurements in the spectral range from 1.5 to 6.5 eV. We analyzed SE experimental data using a CompleteEase software provided by WoollamCo.. We used MSA mode to obtain diagonal elements of the permittivity tensor ε_{1r} and ε_{1i} of CeHfxCoO thin films. In MSA mode, we combined SE and transmission measurements for each CeHfxCoO film composition on both substrates.
c) **Faraday effect spectroscopy:** We studied MO properties of examined samples by MO Faraday effect spectroscopy. We performed this type of measurement only on samples with quartz substrate since these samples are transparent in the whole measured spectral range. Therefore, there was no need for additional MOKE measurement. We acquired all the spectra at room temperature and normal light incidence. We applied magnetic field 670 mT, which was enough for samples saturation. Incident light was p polarized. We recorded data in the photon energy range from 0.7 to 4 eV.

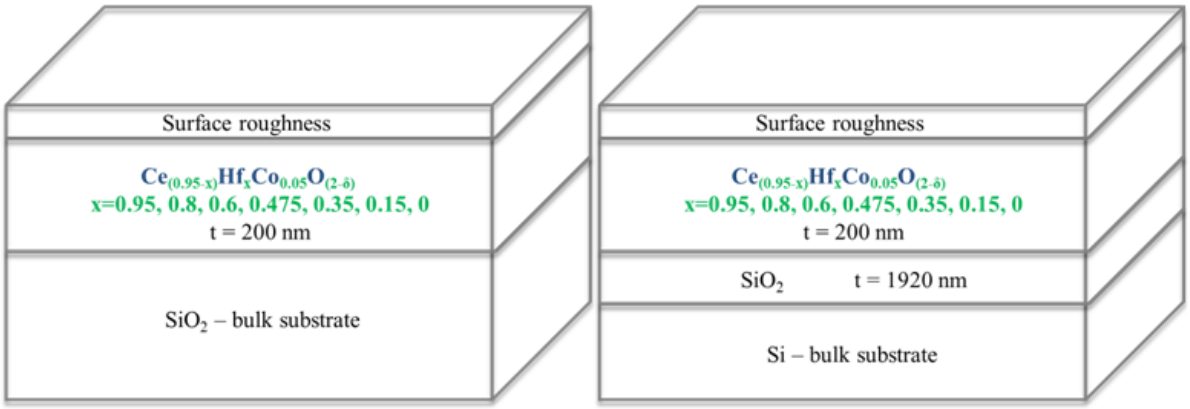

Figure 13: Model structure of CeHfxCoO samples used for SE and Faraday analysis calculations.

In this work, we determined complete permittivity tensors of CeHfxCoO thin films with various Hf concentrations (x= 0, 0.15, 0.35, 0.475, 0.6, 0.8, 0.95) in the spectral range from 1.5 to 5.5 eV. Our analysis showed that Hf content decreases ε_{1r} amplitudes in the whole measured spectral range (Figure 14). We also observed optical bandgap energies to be shifted from 3.21 to 4.1 eV when Hf content increased. We related these energies to O2p -> Ce4f electronic transitions. Similarly, we found that Hf doping decreases absorption in the whole measured spectral range. From this result we assumed that when is Hf replacing Ce in the material; it acts against optical vacancies from isolated Ce4f states localized within the optical bandgap, responsible for enhanced optical absorption. Absorption tail below 3.2 eV supported this theory and it was attributed to the effect of mid-gap defects. When investigating MO properties, we found that Faraday rotation extreme is shifting from 2.9 eV to higher energies. Rotation values decreased when Hf content increased. On the other hand, ellipticity values acted in the opposite manner. We also found that Hf substitution decreases both, ε_{2i} and ε_{2r} amplitudes and it is shifting their maxima to higher energies in the measure spectral range (Figure 15). This was explained by magnetoelastic effects which originate from distortions caused by in-plane compressive strain and vary with Ce-Co content. Hf substitution influences this content and reduces oxygen vacancies important for CeHfxCoO magnetism. We parameterized ε_{2r} and ε_{2i} spectra in terms of microscopic theory by the sum of Para and Dia oscillator terms. We found that the main MO contribution comes from Dia transitions at (1.5-1.65 eV) which refers to localized 4f states in the band gap and at (3.75-4.3 eV) which refers to the oxygen electronic transitions.

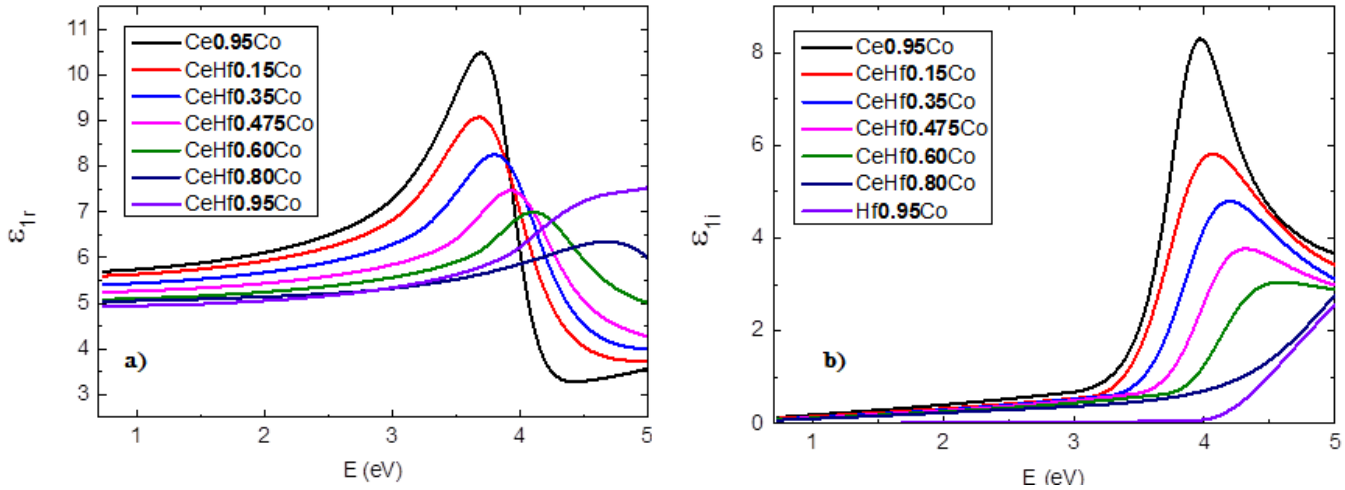

Figure 14: a) Real parts of the diagonal permittivity tensor elements ε1r of CeHfxCoO thin films. b) Imaginary parts of the diagonal permittivity tensor elements ε1i of CeHfxCoO thin films.

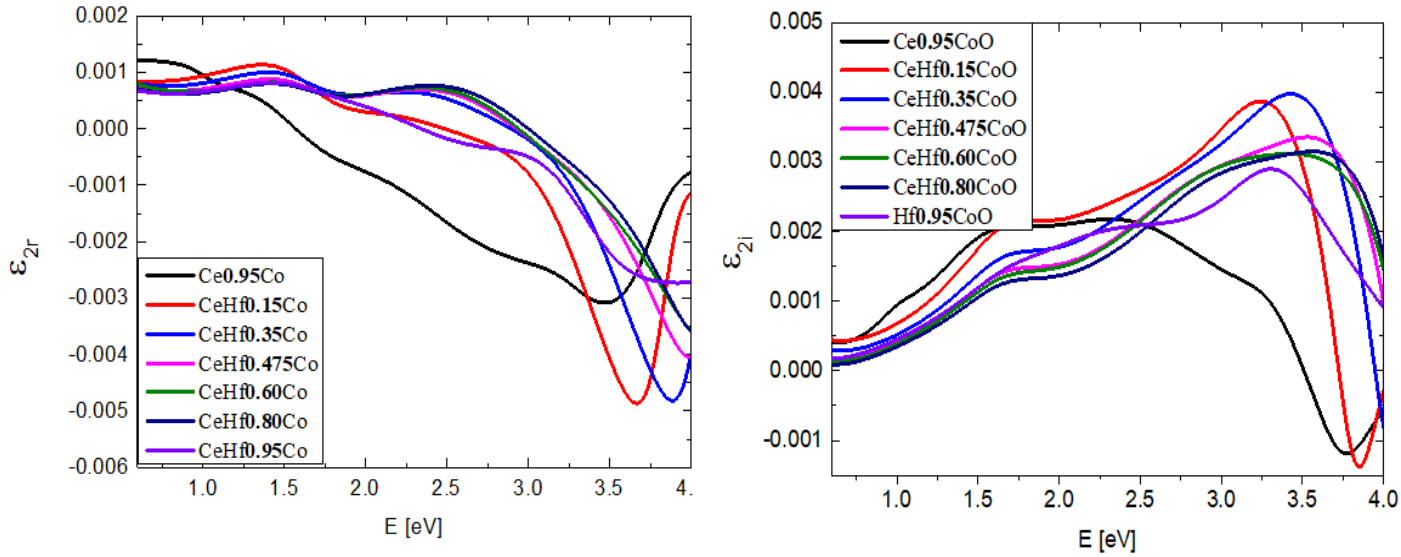

Figure 15: a) Real parts of the off-diagonal permittivity tensor elements ε_{2r} of CeHfxCoO films. b) Imaginary parts of the off-diagonal permittivity tensor elements ε_{2i} of CeHfxCoO films.

List of Abbreviations

MO- Magneto-optical

SE- Spectroscopic Ellipsometry

MOKE- Magneto-optical Kerr Effect

EMA - Effective Medium Approximation method

MSA – Multi Sample Analysis

MOD - Metal Organic Decomposition

MO-SLM – Magneto-optical Spatial Light Modulator

GGG – Gadolinium Gallium Garnet, $Gd_3Ga_5O_{12}$

Bix:YIGs – Bismuth substituted Yttrium Iron Garnets, $Y_{3-x}Bi_xFe_5O_{12}$

Bi1:NIGxGs – Bismuth (1) and Gallium (x) substituted Neodymium Iron Garnets, $Nd_2BiFe_{(5-x)}Ga_xO_{12}$.

Bi2.5:NIGxGs- Bismuth (2.5) and Gallium (x) substituted Neodymium Iron Garnets, $Nd_{0.5}Bi_{2.5}Fe_{(5-x)}Ga_xO_{12}$

CeHfCoO – Hafnium and Cobalt substituted Cerium Oxide, $Ce_{(0.95-x)}Hf_xCo_{0.05}O_{(2-\delta)}$

Bibliography

[1] I. J.A. Woollam Co., CompleteEASE Data Analysis Manual, J.A. Woollam Co., Inc., 2011.

[2] D.D.S. Meneses, M. Malki, P. Echegut, Structure and lattice dynamics of binary lead silicate glasses investigated by infrared spectroscopy, J. Non-Cryst. Solids, 352 (2006) 769–776.

[3] F. Wooten, Optical Properties of Solids, Academinc Press, INC., New York, 1972.

[4] T. E. Tiwald, D. W. Thompson, J. A. Woollam, W. Paulson, R. Hance, Application of IR variable angle spectroscopic ellipsometry to the determination of free carrier concentration depth profiles, Thin Solid Films, 313-314 (1998) 661-666.

[5] P. Yeh, Optics Of Anisotropic Layered Media: A New 4 X 4 Matrix Algebra, Surf. Sci., 96 (1979) 41-53.

[6] F.J. Kahn, P.S. Pershan, J.P. Remeika, Ultraviolet Magneto-Optical Properties of Single-Crystal Orthoferrites, Garnets, and Other Ferric Oxide Compounds, Phys. Rev., 186 (1969) 891-918.

[7] S. Wittekoek, T.J.A. Poprna, J.M. Robertson, P.F. Bongers, Magneto-optic spectra and the dielectric tensor elements of bismuth-substituted iron garnets at photon energies between 2.2—5.2 eV, Phys. Rev. B, 12 (1975) 2777-2788.

[8] D. Schmidt, M. Schubert, Anisotropic Bruggeman Effective Medium Approaches for Slanted Columnar Thin Films, J. Appl. Phys., 114 (2013) 083510 (083511).

[9] N. Imamura, C. Ota, Experimental Study on Magneto-Optical Disk Exerciser with the Laser Diode and Amorphous Magnetic Thin Films, Jpn. J. Appl. Phys., 19 (1980) L731-L734.

[10] K. Aoshima, K. Machida, D. Kato, T. Mishina, K. Wada, Y.-f. Cai, H. Kinjo, K. Kuga, H. Kikuchi, T. Ishibashi, N. Shimidzu, A Magneto-Optical Spatial Light Modulator Driven by Spin Transfer Switching for 3D Holography Applications, J. Disp. Technol., 11 (2015) 129-135.

[11] S. Mangin, G. Marchal, C. Bellouard, W. Wernsdorfer, B. Barbara, Magnetic behavior and resistivity of the domain-wall junction GdFe(1000 Å)/TbFe/GdFe(500 Å)..Phys. Rev. B, 58 (1998) 2748-2757.

[12] N. Nishimura, T. Hirai, A. Koganei, T. Ikeda, K. Okano, Y. Sekiguchi, Y. Osada, Magnetic tunnel junction device with perpendicular magnetization films for high-density magnetic random access memory, J. Appl. Phys., 91 (2002) 5246.

[13] M. Urner-Wille, K. Witter, Compensation point switching in homogeneous amorphous GdFe-films, J. Magn. Magn. Mater., 13 (1979) 77-80.

[14] Z. Shen, J. Li, S. Wang, S. Zhou, L. Chen, Magneto-optical and optical properties of GdFe films, in: F. Gan, L. Hou (Eds.) Fifth International Symposium on Optical Storage, SPIE, Shanghai, 2000, pp. 76-79.

[15] S. Sugano, N. Kojima, Magneto-Optics, Springer, Japan, 2011.

[16] L. Boernstein, Magnetic Properties of Metals, Springer-Verlag, Tokyo, 1986.

[17] H. Kinjo, K. Machida, K. Matsui, K.-i. Aoshima, D. Kato, K. Kuga, H. Kikuchi, N. Shimidzu, Low-current-density spin-transfer switching in Gd22Fe78-MgO magnetic tunnel junction, J. Appl. Phys., 115 (2014) 203903.

[18] K. Aoshima, Y. Hashimoto, N. Funabashi, K. Machida, K. Kuga, H. Kikuchi, N. Shimidzu, T. Ishibashi, Spin transfer switching of current-perpendicular-to-plane giant magnetoresistance with various Gd-Fe free-layer compositions, J. Appl. Phys., 111 (2012) 07C911.

[19] A. Quemerais, B. Loisel, G. Jezequel, J. Thomas, J.C. Lemonnier, Optical spectra of gadolinium and dysprosium: study of the 5p thresholds, J. Phys. F: Met. Phys., 11 (1981) 293-303.

[20] E.D. Palik, Handbook of Optical Constants of Solids, Accademic Press, 1991.

[21] A. Kirihara, K.-I. Uchida, Y. Kajiwara, M. Ishida, Y. Nakamura, T. Manako, E. Saitoh, S. Yorozu, Spin-current-driven thermoelectric coating, Nat. Mater., 11 (2012) 686-689.

[22] H. Nakayama, M. Althammer, Y.-T. Chen, K. Uchida, Y. Kajiwara, D. Kikuchi, T. Ohtani, S. Geprags, M. Opel, S. Takahashi, R. Gross, G.E.W. Bauer, S.T.B. Goennenwein, E. Saitoh, Spin Hall Magnetoresistance Induced by a Nonequilibrium Proximity Effect, Phys. Rev. Lett., 110 (2013) 206601(206605).

[23] T. Ishibashi, K. Kawata, T.H. Johansen, J. He, N. Harada, K. Sato, Magneto-optical Indicator Garnet Fimls Grown by Metal-organic Decomposition Method, J. Phys. Soc. Jpn., 32 (2008) 150-153.

[24] T. Ishibashi, T. Kosaka, M. Naganuma, T. Nomura, Magneto-optical properties of Bi-substituted yttrium iron garnet films by metal-organic decomposition method, in: International Conference on Magnetism (ICM 2009), IOP Publishing, 2009, pp. 112002 (112004).

[25] L. Bi, J. Hu, P. Jiang, D.H. Kim, G.F. Dionne, L.C. Kimerling, C.A. Ross, On-chip optical isolation in monolithically integrated non-reciprocal optical resonators, Nat Photon, 5 (2011) 758-762.

[26] M. Inoue, H. Uchida, K. Nishimura, P.B. Lim, Magnetophotonic crystals-a novel magneto-optic material with artificial periodic structures, Journal of Materials Chemistry, 16 (2006) 678-684.

[27] K. Iwasaki, H. Mochizuki, H. Umezawa, M. Inoue, Practical Magneto-Optic Spatial Light Modulator With Single Magnetic Domain Pixels, IEEE Trans. Magn., 44 (2008) 3296-3299.

[28] M. Pohl, L.E. Kreilkamp, V.I. Belotelov, I.A. Akimov, A N. Kalish, N.E. Khokhlov, V.J. Yallapragada, A.V. Gopal, M. Nur-E-Alam, M. Vasiliev, D.R. Yakovlev, K. Alameh, A K. Zvezdin, M. Bayer, Tuning of the transverse magneto-optical Kerr effect in magneto-plasmonic crystals, New Journal of Physics, 15 (2013) 075024.

[29] A. Tiwari, V.M. Bhosle, S. Ramachandran, N. Sudhakar, J. Narayan, S. Budak, A. Gupta, Ferromagnetism in Co doped CeO2: Observation of a giant magnetic moment with a high Curie temperature, Appl. Phys. Lett., 88 (2006) 142511.

[30] V. Fernandes, J.J. Klein, N. Mattoso, D.H. Mosca, E. Silveira, E. Ribeiro, W.H. Schreiner, J. Varalda, A.J.A. de Oliveira, Room temperature ferromagnetism in Co-doped CeO2 films on Si(001), Phys. Rev. B, 75 (2007) 121304.

[31] B. Vodungbo, Y. Zheng, F. Vidal, D. Demaille, V.H. Etgens, D.H. Mosca, Room temperature ferromagnetism of Co doped CeO2−δ diluted magnetic oxide: Effect of oxygen and anisotropy, Appl. Phys. Lett., 90 (2007) 062510.